Proceedings of the ASME 2024
Pressure Vessels & Piping Conference
PVP2024
July 29–August 2, 2024, Bellevue, Washington

PVP2024-123184

INFLUENCE OF RESONANT ACOUSTIC MODE SHAPE ON SOURCE AND SINK PATTERNS IN THE WAKE OF A SINGLE CYLINDER BASED ON HOWE'S ENERGY COROLLARY

Mahmoud Shaaban[1,2,*], Mostafa R. Rashed[3], Atef Mohany[4]

[1]School of Engineering and Applied Sciences, Nile University, Giza, Egypt
[2]Smart Engineering Systems Center, Nile University, Giza, Egypt
[3]Mechanical Engineering Department, Faculty of Engineering, Modern University for Technology and Information, Cairo, Egypt
[4]Ontario Tech University, Oshawa, ON, Canada

ABSTRACT

The interaction between the acoustic field and periodic flow structures in the wake of a cylinder can self-excite resonance and lead to undesirable noise and vibrations in heat exchangers. The underlying energy exchange mechanism responsible for the emergence of a resonant acoustic field depends on the coupling between flow and acoustic parameters in time and space. Previous investigations have demonstrated that a net positive acoustic energy rate over a complete coupled cycle is essential to sustain resonant conditions. However, existing models have primarily focused on the excitation of the fundamental acoustic mode, considering only one-way coupling, resulting in predominantly qualitative findings. This study utilizes Howe's energy corollary to determine the amount of acoustic energy produced and absorbed by the flow moving downstream of a single cylinder in a rectangular duct. By considering full coupling, resonant mode shapes are self-excited, enabling the computation of the acoustic and flow fields, acoustic energy generation, and the phase delay between the acoustic field and the lift force. Results provide detailed insights into the coupling mechanism governing the first three transverse acoustic modes, which can be excited by the unsteady vorticity shedding from the cylinder within the relevant velocity range of interest.

NOMENCLATURE

Parameters

D	Cylinder diameter
H	Channel height
M	Mach number
P	Acoustic power
St	Strouhal number
W	Channel width
f	Frequency
k	Turbulence kinetic energy
p	Static pressure
t	Time
$\boldsymbol{u}$	Velocity vector
Π	Acoustic power generation rate
$\overline{\tau}$	Shear tensor
ϕ	Velocity potential
ρ	Fluid density
$\omega, \boldsymbol{\omega}$	Turbulence dissipation rate, vorticity vector; respectively

Abbreviations

GCI	Grid convergence index
M	Mesh
SST	Shear stress transport

Superscripts and subscripts

0	Stagnation
a	Acoustic
avg	Average
f	Flow
$inst$	Instantaneous
irr	Irrotational
r	Reduced
∞	Upstream
$*$	Normalized

1. INTRODUCTION

The generation of acoustic energy by fluid flow can lead to sustained noise and vibration problems, with negative implications in several industrial applications such as heat exchangers [1, 2], combustors [3], external flow [4], ventilation ducts [5], and many others. The basic mechanism of flow-excited acoustic resonance has been explored in a series of studies on different configurations, such as cylinder arrangements [6, 7], tube banks [8], cavities [9, 10], and side branches [11]. In its simplest form, a

*Corresponding author: mashaaban@nu.edu.eg

Copyright © 2024 by ASME

coupling between the acoustic and flow fields is initiated when the frequency of a periodic flow instability approaches an excitable acoustic mode, and the flow energy is higher than the acoustic losses in the system. These instabilities drive acoustic fluctuations, which, in turn, organize the flow structures and lead to an alignment of phases between the two fields. This feedback drives a lock-in condition in which both frequencies become equal with a constant phase between them, leading to a net energy transfer from the flow to the acoustic field. As a result, the growing acoustic field sustains high sound pressure that may reach its limit cycle at extreme conditions [12]. Although the general details of the coupling mechanism are well known, many of the intricate details required to understand and manipulate it are still being researched.

Much research has been done on how vortex shedding can cause an acoustic resonance in the case of isolated cylinders in ducted cross-flow [13]. Experimental investigations asserted that a high correlation between vortex shedding and the acoustic cycle is vital to initiating and sustaining resonance [14]. Mohany and Ziada [15] experimentally measured the dynamic lift forces on cylinders, showing that acoustic resonance is associated with a clear synchronization of the acoustic oscillations and the fluid forces. Moreover, Hanson et al. [16] and Mohany et al. [17] showed that resonance could synchronize vortex shedding between side-by-side cylinders in proximity flow interference. Later, a series of investigations by Shaaban and Mohany[18] showed that acoustic resonance could drive a similar synchronization between cylinders at a large aerodynamically isolated spacing. Quantifying energy exchange during the acoustic cycle was possible with detailed flow field visualizations. This showed the basic direction of energy transfer around the cylinders during the acoustic cycle [19]. Recently, they used high-frequency phase-resolved flow field measurements to figure out how the resonant acoustic field affected the movement of vortex shedding in the wake of three separate cylinders [18]. Although much has been learned from experimental studies, limitations on the spatial scale and frequency of particle image velocimetry raise the need for numerical studies to extend the current knowledge scope.

Over the past two decades, computational aeroacoustic simulations have been extensively employed in various industrial applications to predict noise levels [20]. Numerical simulations are well-suited for modeling a variety of coupled physics phenomena, encompassing applications such as flow-induced vibration [21], radioactive flow [22], and other multiphysics applications. Consequently, they have been extensively utilized for the purpose of predicting noise production in turbulent flows and elucidating the associated vortical structures within these flow fields [23]. Numerical-based methods are appealing for this purpose as they offer an invaluable tool to visualize the full field, whose measurements are tedious and sometimes unfeasible to design due to the disparity in the dynamic time scales. Although the effect of resonance excitation on the structure of vortices has been successfully inspected in a compressible 2D simulation by Mohany and Ziada [24], the coupling was enforced and seeded by information from experimental runs. Further attempts to predict the acoustic pressure from simulation have been largely dependent on adjusting the vortex shedding phasing with the lift force or imposing a forcing term manually [17]. The coupled dynamics require extensive manipulation to explore the two fields and their interactions. In terms of density, Lighthill's analogy turns the compressible Navier-Stokes equations into an inhomogeneous wave equation. This model shows how energy moves between flow fields and acoustic fields [25]. Howe [26] simplified the method for use in low-Mach flows dominated by vortex shedding, allowing him to predict the acoustic energy absorption resulting from the vortex shedding in organ pipes. Recently, Hong et al.[27] showed that vortex-sound interaction can be captured through nonlinear theoretical meshless models without imposing an external phasing, albeit with a lower quantitative precision. Nevertheless, no purely numerical models have been reported to predict the mechanism of acoustic resonance and explore the interaction between the acoustic and flow fields. Such progress can provide an invaluable tool for designers and complement experimentation and modeling.

In this work, we aim to establish a numerical model that fully accounts for the unsteady flow field, the unsteady acoustic field, and their coupling to estimate the acoustic generation by vorticity shedding at lock-in conditions. First, the compressible fluid flow equations are solved with an unsteady Reynolds-Stress turbulence model at a time resolution sufficient for the acoustic cycles to be developed and a space resolution sufficient to model the unsteady flow separation and reattachment cycles accurately. The acoustic fields are decomposed through a Helmholtz decomposition to separate the irrotational acoustic and rotational flow quantities, such that Howe's corollary is applied to provide an estimation of the sound generation and absorption, which is then averaged to explore the noise production mechanism. The estimated root-mean-squared acoustic pressure is extracted and compared to experimental studies for validation. Subsequently, the details of the acoustic pressure and particle velocity fields at the peak of the first and third acoustic modes are inspected for the first time.

2. METHODOLOGY

2.1 Governing equations

In this paper, the 2D compressible unsteady RANS formulation of the Navier-Stokes equation is adopted to reproduce the flow field and the aerodynamic sound of the flow in the vicinity of a single circular cylinder in cross-flow. The simulation is carried out at Reynolds numbers ranging from 5×10^4 to 20×10^4 based on the cylinder diameter. The continuity and Navier-Stokes equations for compressible flow can be written as follows:

$$\frac{\partial \rho}{\partial t} + \nabla \cdot (\rho \boldsymbol{u}) = 0 \tag{1}$$

$$\frac{\partial}{\partial t}(\rho \boldsymbol{u}) + \nabla \cdot (\rho \boldsymbol{u} \cdot \boldsymbol{u}) = -\nabla p + \nabla \cdot \left(\bar{\bar{\tau}}\right) \tag{2}$$

where ρ is the density, calculated from the ideal gas relation, and $\bar{\bar{\tau}}$ is the shear stress tensor. The Shear Stress Transport (SST) k- ω model [28] is used to consider the effect of turbulence in the region of vortex shedding. The model is based on transport equations for the turbulence kinetic energy k and the specific dissipation rate ω.

Figure 1 shows the computational domain used in this work. These dimensions are similar to those in experimental works for

Copyright © 2024 by ASME

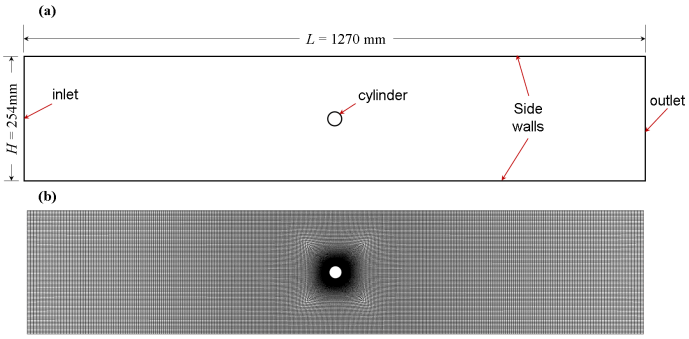


FIGURE 1: (A) THE COMPUTATIONAL DOMAIN, AND (B) THE COMPUTATIONAL GRID.

ease of comparison [6, 18, 29, 30]. The height of the flow channel is set at $H = 254$ mm, and the first acoustic transverse mode frequency is around 675 Hz. Two different diameters, $D = 25.4$ mm and 12.7 mm, were used to enable vortex shedding frequencies in the range of the first three acoustic mode frequencies. The length of the domain was extended to $L = 1.27$ m, equivalent to $5H$ and $100D$ for the larger diameter extending equal distances upstream and downstream of the cylinder, sufficient to eliminate significant edge effects on the major acoustic mode and vortex shedding [10].

The iterative PISO solver computes the pressure, velocity, and density fields every time step through a series of iterations that are required to converge to residuals of 10^{-4} at most. Second-order numerical discretization of the convection and flux terms is used to ensure stability and accuracy. A time step of 10^{-5} s is used at all flow velocities. This value ensures at least 150 points per acoustic cycle and, therefore, provides an accurate resolution of the acoustic cycle as well as the flow quantities. The normalized acoustic pressure is calculated from the root-mean-square of the absolute pressure signal using equation 3.

$$p^* = p_{\text{rms}}/0.5\rho U_\infty^2 M \tag{3}$$

The frequency of the oscillating pressure signal f_a is calculated via a power spectral density analysis, while the vortex shedding frequency f is calculated as the oscillating frequency of the lift force signal.

To identify the acoustic velocity field, a Helmholtz decomposition is performed following the strategy developed by De Roeck and Desmet [31]. The decomposition isolates the irrotational and the rotational components of the velocity $\boldsymbol{u}$ that allow the study of the specific properties of vortex dynamics and acoustic modes using the potential representation.

In this work, a scalar potential formulation similar to that implemented by Schoder et al. [32] is used to solve the Poisson equation:

$$\nabla \cdot \nabla\phi = \nabla \cdot \boldsymbol{u} \tag{4}$$

where ϕ is the scalar potential associated with the compressible component of the flow at a low Mach number. The decomposed components obtained include the harmonic component due to the boundary values of the partial differential equation. By carefully adjusting the boundary conditions such that the harmonic part is separated from the compressible part, the Helmholtz decomposition results in

TABLE 1: BOUNDARY CONDITIONS

	inlet	walls	outlet
$\boldsymbol{u}$	$\boldsymbol{u} = U_\infty \boldsymbol{i}$	$\boldsymbol{u} = 0$	$\boldsymbol{u} \cdot \boldsymbol{n} = 0$
p	$p \cdot \boldsymbol{n} = 0$	$p \cdot \boldsymbol{n} = 0$	$p = 0$
$\boldsymbol{k}$	$k = 10^{-5} U_\infty / Re_H$	$k \cdot \boldsymbol{n} = 0$	$k \cdot \boldsymbol{n} = 0$
ω	$\omega_\infty = 10 U_\infty / H$	$\omega = 60 U_\infty / 0.075 y_w^2$	$\omega \cdot \boldsymbol{n} = 0$
ϕ	$\phi = 0$	$\phi \cdot \boldsymbol{n} = 0$	$\phi = 0$

$$\nabla\phi = \boldsymbol{u}_a \tag{5}$$

In this work, equation 4 is solved as an additional equation coupled with the system of Navier-Stokes equations 1 and 2. As a transport equation, the equation is solved for an additional scalar potential ϕ. The source term is the flow velocity gradient calculated from the Navier-Stokes equations, and no convective flux term is included. Once the value of ϕ converges, the acoustic velocity can be calculated as its gradient, allowing the calculation of the aerodynamic velocity $\boldsymbol{u}_f$ according to equation 6. The boundary conditions set for the domain are listed in table 1.

$$\boldsymbol{u}_f = \boldsymbol{u} - \boldsymbol{u}_a \tag{6}$$

The integral formula in equation 7 proposed by Howe [33] is used to estimate the volumetric rate of energy exchanged between the flow field and the acoustic modes. A rate of energy Π is transferred from the fluid field to the acoustic field in a region where the vectors of Coriolis force density $\rho_0 (\boldsymbol{\omega} \times \boldsymbol{u}_f)$ and the acoustic particle velocity u_a are highly correlated, such that:

$$\Pi = -\frac{1}{2}\rho_0 \frac{\partial}{\partial t} \int\int\int u_{irr}^2 dV \approx -\rho_0 \int\int\int_V (\boldsymbol{\omega} \times \boldsymbol{u}_f) \cdot \boldsymbol{u}_a dV \tag{7}$$

where u_{irr} is the irrotational velocity component. In this work, the flow and acoustic components are readily available from the solution of equations 5 and 6. The vorticity ω is calculated as the curl of the flow velocity using central differencing, and the density field ρ_0 is obtained from the ideal gas relation. The field of the instantaneous acoustic power volumetric source is then calculated according to the sign convention as in equation 8 [34]:

$$P = -\rho_0 (\boldsymbol{\omega} \times \boldsymbol{u}_f) \cdot \boldsymbol{u}_a \tag{8}$$

To quantify sound generation by the coupling mechanism, the net generation of acoustic power is calculated by an ensemble average over ten acoustic cycles.

2.2 Mesh sensitivity analysis

The spatial mesh convergence was assessed using the methodology proposed by Roache [35]. The evaluation is based on the Grid Convergence Index (GCI), which is derived using an error estimator from the theory of generalized Richardson extrapolation. The GCI offers a quantitative measure of the uncertainty

Copyright © 2024 by ASME

TABLE 2: MESH SENSITIVITY ANALYSIS FOR A CIRCULAR CYLINDER OF D = 25 mm, AND UPSTREAM FLOW VELOCITY OF U_∞ = 82 m/s

Mesh	Number of elements	Average mesh spacing	$C_{l,\text{rms}}$
M1	25,423	4.377	2.060
M2	45,762	2.432	2.035
M3	82,372	1.351	2.022

associated with mesh convergence, indicating the percentage difference between the calculated and the asymptotic numerical values. To compute the GCI, three mesh setups, M1, M2, and M3, as tabulated in table 2 with a refinement ratio $r_{12} = 1.8$ were used. The GCI analysis showed that mesh setup M2 yielded satisfactory results with a minimal error of less than 0.9%.

3. RESULTS AND DISCUSSIONS

3.1 Generated acoustic pressure

Figure 2 presents the prediction of the aeroacoustic response of a single cylinder compared with experimental works for two different reduced velocity ranges representing two different acoustic modes. In figure 2a, the root mean square values of the pressure are presented in their absolute form for a cylinder with a diameter of 25.4 mm during excitation of the first acoustic mode. The numerical simulation predicts a remarkable value of around 2 kPa, which is close to the experimental value of 2.5 kPa. The lock-in region width is also well predicted. On the other hand, the numerical simulation predicted resonance at a slightly lower flow velocity, reaching the peak at reduced flow velocities about 10% lower than those observed during the simulation. With careful inspection, the Strouhal number predicted by the simulation is around 0.22 for the range of flow velocities considered. This behavior is typical for 2D URANS simulations, where the $k-\omega$ SST model tends to overestimate the Strouhal number of vortex shedding [36].

The oscillating pressure in figure 2a is shown in its normalized form to account for the difference in cylinder diameter. At the velocity of frequency coincidence corresponding to the third acoustic mode ($St \times U_r \approx 3$), acoustic resonance is excited. While the flow velocity at resonance suffers the same shift as in the first acoustic mode for the same overestimation of the Strouhal number, the normalized acoustic pressure is well predicted. Because accurate information regarding the Strouhal number is available from a large body of literature, the shift in flow velocity can be reasonably corrected, and the information provided in the resonance prediction can thus be considered useful.

The simulations carried out for the full reduced velocity range are presented in figure 3. The figure shows that the simulation was capable of capturing the trend of the aeroacoustic response observed in experiments. At around $St \times U_r = 1$, the first mode excitation can be observed where the acoustic pressure increases significantly and the frequency of the lift force, related to vortex shedding, locks in the fixed value of the first acoustic mode frequency of f_a = 683 Hz. As the reduced flow velocity is increased, the lock-in recedes, and the vortex shedding reverts back to the linear Strouhal relationship, with a proportionality constant of around 0.21. Notably, no resonance is observed at the flow velocities expected to excite the second mode (i.e., $St \times U_r \approx 2$). This reflects an accurate behavior in agreement with Arafa and Mohany [30]. At much higher reduced velocities where $St \times U_r \approx 3$, the third mode is excited, and another episode of frequency lock-in is observed.

3.2 Flow field characteristics

Figure 4 shows the vorticity fields at instants during the strong oscillations of the first and third acoustic mode excitations. As expected, the normalized vorticity values are comparable directly downstream of both cylinders. On the other hand, vortex cores are maintained to a higher distance downstream for the larger cylinder at the higher flow velocity, and turbulence leads to a deterioration of the vortex cores at U_∞ = 115 m/s. During the excitation of the first acoustic transverse mode, a pair of vortices is shed downstream, compared with the single vortex for the third acoustic cross-mode. The shedding of a pair of vortices is typically associated with strong transverse oscillations of the cylinder relative to the flow, similar to that observed during cylinder vibration. This suggests that the acoustic field is creating an analogous effect, with the flow field moving with a significant transverse flow velocity relative to the cylinder, with a pressure amplitude of over 1 kPa.

The pressure fields shown in figure 5 complement this observation, as the acoustic pressure distribution asserts a dominance of two different acoustic modes. At U_∞ = 82 m/s, the reduced velocity is close to U_r = 5, which is capable of exciting the first acoustic cross-mode of the duct. The pressure distribution in figure 5 is that of a first transverse mode, with antinodes at the two side walls and a single node close to the middle of the domain around the vortex street. In contrast, the third acoustic mode shows not only three nodes in the transverse direction directly downstream of the cylinder but also interacts with longitudinal mode shapes, with a two-dimensional complex mode shape. The exact mode shape will change with the domain extent, and distinguishing the effects of the third pure acoustic transverse mode would require a prohibitively long computational domain. However, the interaction does not cause much distortion to the mode shape in the immediate wake, up to 20 diameters downstream of the cylinder, where the peak of pressure is observed. It is important to note that experimental investigations suffer from the same limitations due to radiation at the ends of the domain. However, this effect is not detrimental to the critical parameter, which is the peak pressure level observed in the immediate vicinity of the cylinder [30].

3.3 Acoustic energy generation

The fields of acoustic energy generation rates calculated from equation 8 provide the fields in figure 6 when applied to the same instances shown in the figures above. The field asserts the fact that the acoustic generation is mainly in action within the street of vortices downstream. The strongest generation rates are evident directly downstream of the cylinder, and the point sources weaken as they are convected downstream. For the first mode,

Copyright © 2024 by ASME

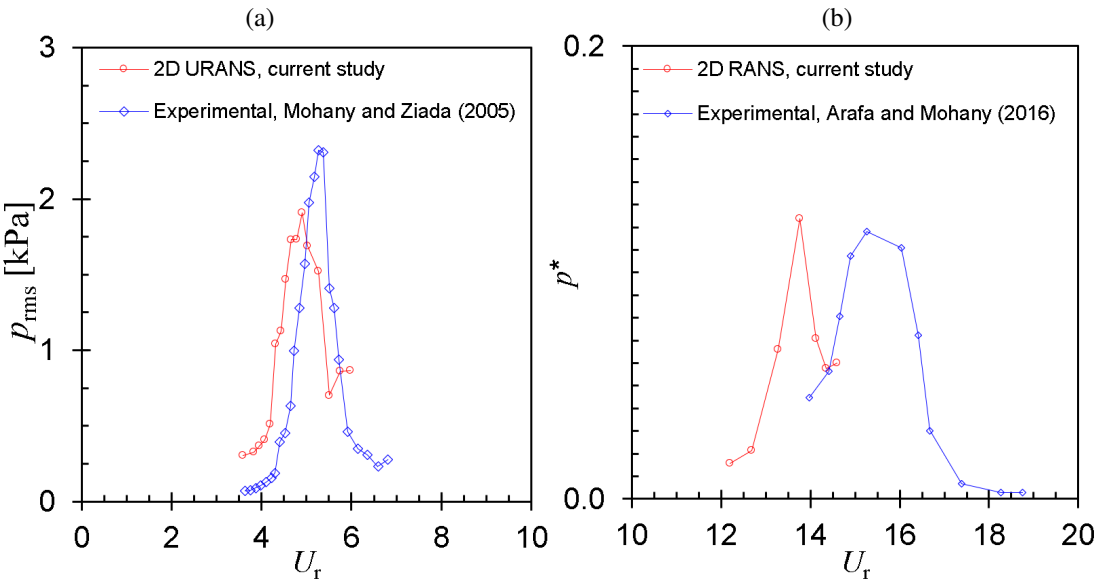


FIGURE 2: A COMPARISON BETWEEN THE RESULTS FROM THE CURRENT STUDY WITH THE EXPERIMENTAL DATA FROM LITERATURE [6, 30], (A) THE ROOT MEAN SQUARE PRESSURE p_{rms} OF THE FIRST ACOUSTIC MODE, (B) AND THE INSTANTANEOUS NORMALIZED ACOUSTIC PRESSURE p^* OF THE THIRD ACOUSTIC MODE.

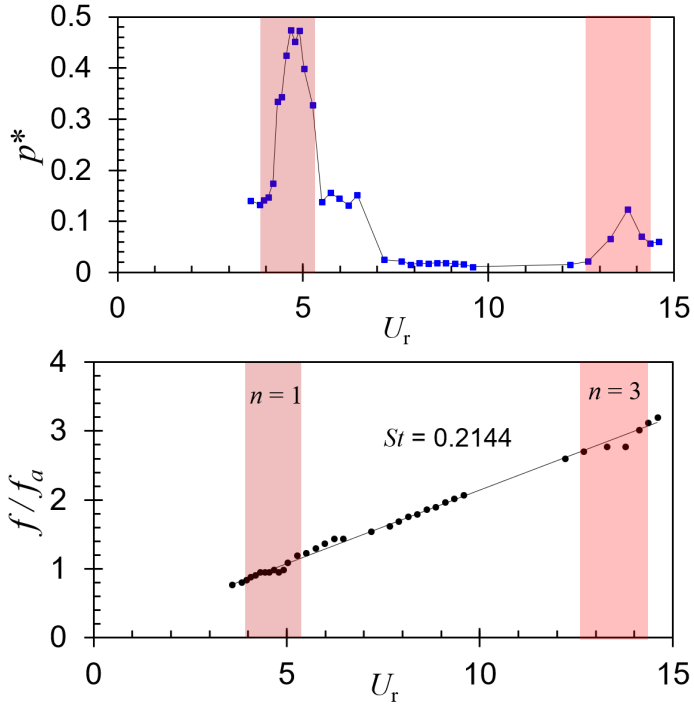


FIGURE 3: THE NORMALIZED ACOUSTIC PRESSURE p^* AND THE RATIO OF VORTEX SHEDDING AND ACOUSTIC FREQUENCY AT DIFFERENT REDUCED VELOCITIES.

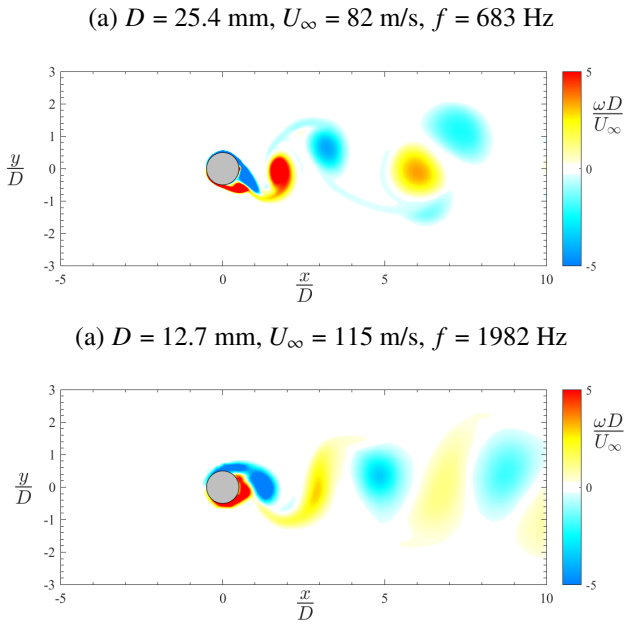


FIGURE 4: THE NORMALIZED FLOW IN-PLANE VORTICITY $\omega D/U_\infty$ AT THE PEAK OF (A) THE FIRST TRANSVERSE ACOUSTIC MODE, AND (B) THE THIRD TRANSVERSE ACOUSTIC MODE

the degradation of the energy transfer is gradual, contributing to a stronger and more uniform acoustic field.

Figure 7 shows the results of ensemble averaging of the acoustic generation rates over ten acoustic cycles. The result is a pattern of alternating sources and sinks extending downstream of the cylinder. Most of the net energy generation occurs directly

Copyright © 2024 by ASME

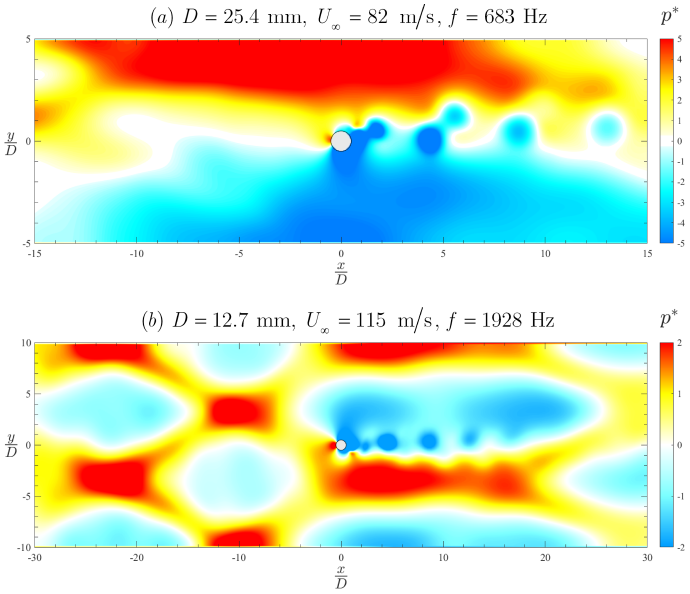


FIGURE 5: THE INSTANTANEOUS NORMALIZED ACOUSTIC PRESSURE p^* AT THE PEAK OF (A) THE FIRST AND (B) THE THIRD TRANSVERSE ACOUSTIC MODES.

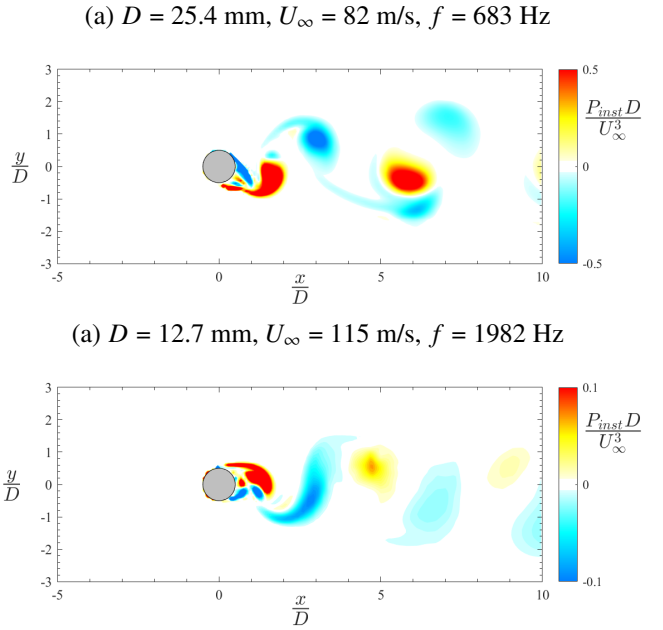


FIGURE 6: THE INSTANTANEOUS NORMALIZED ACOUSTIC ENERGY GENERATION $P_{inst}D/U_\infty{}^3$ AT THE PEAK OF (A) THE FIRST AND (B) THE THIRD TRANSVERSE ACOUSTIC MODES.

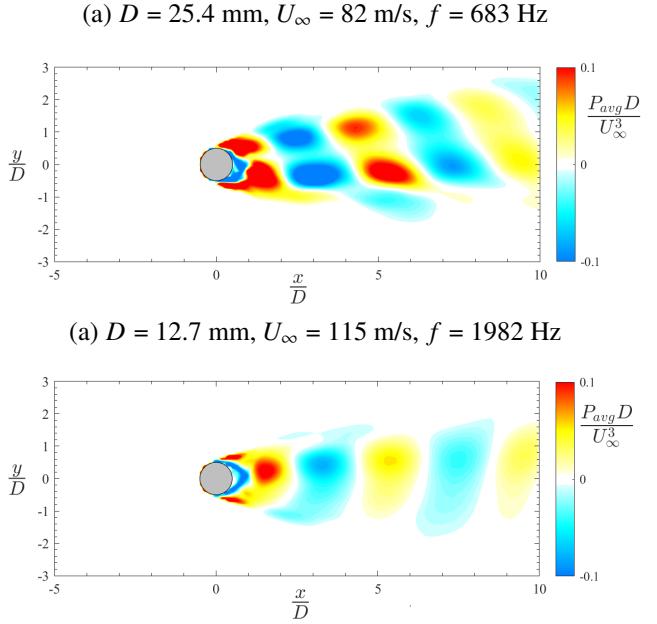


FIGURE 7: THE ENSEMBLE-AVERAGE OF THE NORMALIZED ACOUSTIC ENERGY GENERATION $P_{avg}D/U_\infty{}^3$ AT THE PEAK OF (A) THE FIRST AND (B) THE THIRD TRANSVERSE ACOUSTIC MODES.

downstream of the cylinders, while the region of the source gets stretched downstream. The resulting trend is a valuable method for exploring the spatial and temporal energy interactions within the field and proves that the method implemented here is a powerful analysis tool.

4. CONCLUSION

In this work, a fully coupled numerical model is developed using a two-dimensional compressible formulation to estimate the acoustic resonance induced by the wake flow of a circular cylinder within a duct. As the flow field is calculated, the model decomposes the field into an irrotational sound field and rotational aerodynamic oscillations and simultaneously calculates the energy production from the coupled mechanism. The typical aeroacoustic response of the acoustic resonance in the first and third acoustic modes is well predicted. The developed method reasonably predicts the acoustic and flow fields, the sound source distribution downstream of the cylinder, and the sound pressure within the duct. In addition, the acoustic pressure during acoustic resonance excitation and the frequency lock-in phenomena are well captured, indicating that the underlying mechanisms are resolved. The Strouhal number of the free vortex shedding and the inherent frequency of the acoustic modes are validated by previous experimental data. Although a shift in the resonance peak is observed as the turbulence model inherently overestimates the Strouhal number slightly, both the absolute and the normalized acoustic pressure values agree well with experimental data. Results indicate that higher acoustic mode shapes in the streamwise direction may be possible without imparting from the lock-in mechanism. Such an observation is neither asserted nor refuted in experimental reports and thus requires further inspection, as it

Copyright © 2024 by ASME

is critical to how acoustic resonance is initiated for higher acoustic modes.

REFERENCES

[1] Ziada, Samir. "Flow-Excited Acoustic Resonance in Industry." *Journal of Pressure Vessel Technology* Vol. 132 (2010). DOI 10.1115/1.4000379.

[2] Alziadeh, Mohammed and Mohany, Atef. "Flow structure and aerodynamic forces of finned cylinders during flow-induced acoustic resonance." *Journal of Fluids and Structures* Vol. 119 (2023): p. 103887. DOI 10.1016/j.jfluidstructs.2023.103887.

[3] Britto, Abraham Benjamin and Mariappan, Sathesh. "Self-excited vortex-acoustic lock-in in a bluff body combustor." *Journal of Fluid Mechanics* Vol. 975 (2023): p. A16. DOI 10.1017/jfm.2023.845.

[4] Shaaban, Mahmoud and Mohany, Atef. "Flow–acoustic coupling around rectangular rods of different aspect ratios and incidence angles." *Experiments in Fluids* Vol. 63 (2022): p. 45. DOI 10.1007/s00348-022-03380-2.

[5] Ravichandran, Asvath, Logdesser, Andreas, Peller, Nikolaus and Manhart, Michael. "Acoustic resonances in an automotive HVAC outlet." *Journal of Sound and Vibration* Vol. 569 (2024): p. 118051. DOI 10.1016/j.jsv.2023.118051.

[6] Mohany, Atef and Ziada, Samir. "Flow-excited acoustic resonance of two tandem cylinders in cross-flow." *Journal of Fluids and Structures* Vol. 21 (2005): pp. 103–119. DOI 10.1016/j.jfluidstructs.2005.05.018.

[7] Islam, Mohammad Rashidul, Shaaban, Mahmoud and Mohany, Atef. "Vortex dynamics and acoustic sources in the wake of finned cylinders during resonance excitation." *Physics of Fluids* Vol. 32 (2020). DOI 10.1063/5.0016076.

[8] Mohany, Atef, Alziadeh, Mohammed and Hassan, Marwan. "Vorticity Shedding and Acoustic Resonance Excitation of a Square Tube Array: Effect of Flow Approach Angle." *Journal of Pressure Vessel Technology* Vol. 145 (2023). DOI 10.1115/1.4055158.

[9] Abdelmwgoud, Moamenbellah, Shaaban, Mahmoud and Mohany, Atef. "Flow dynamics and azimuthal behavior of the self-excited acoustic modes in axisymmetric shallow cavities." *Physics of Fluids* Vol. 32 (2020). DOI 10.1063/5.0026552.

[10] Abdelmwgoud, Moamenbellah, Shaaban, Mahmoud and Mohany, Atef. "Shear layer synchronization of aerodynamically isolated opposite cavities due to acoustic resonance excitation." *Physics of Fluids* Vol. 33 (2021). DOI 10.1063/5.0051226.

[11] Wang, Peng, He, Li and Liu, Yingzheng. "Acoustics-driven vortex dynamics in channel branches with round intersections: Flow mode transition and three-dimensionality." *Physics of Fluids* Vol. 32 (2020). DOI 10.1063/1.5141609.

[12] Weaver, David S., Taylor, Colette E. and Pettigrew, Michel J. *Periodic Wake Shedding and Acoustic Resonance*. Wiley (2021): pp. 329–372. DOI 10.1002/9781119810995.ch11.

[13] Mohany, Atef. "Self-Excited Acoustic Resonance of Isolated Cylinders in Cross-Flow." *AECL Nuclear Review* Vol. 1 (2012): pp. 45–55. DOI 10.12943/ANR.2012.00007.

[14] Ziada, Samir and Lafon, Philippe. "Flow-Excited Acoustic Resonance Excitation Mechanism, Design Guidelines, and Counter Measures." *Applied Mechanics Reviews* Vol. 66 (2014). DOI 10.1115/1.4025788.

[15] Mohany, Atef and Ziada, Samir. "Effect of acoustic resonance on the dynamic lift forces acting on two tandem cylinders in cross-flow." *Journal of Fluids and Structures* Vol. 25 (2009): pp. 461–478. DOI 10.1016/j.jfluidstructs.2008.08.007.

[16] Hanson, Ronald, Mohany, Atef and Ziada, Samir. "Flow-excited acoustic resonance of two side-by-side cylinders in cross-flow." *Journal of Fluids and Structures* Vol. 25 (2009): pp. 80–94. DOI 10.1016/j.jfluidstructs.2008.03.008.

[17] Mohany, Atef, Arthurs, David, Bolduc, Michael, Hassan, Marwan and Ziada, Samir. "Numerical and experimental investigation of flow-acoustic resonance of side-by-side cylinders in a duct." *Journal of Fluids and Structures* Vol. 48 (2014): pp. 316–331. DOI 10.1016/j.jfluidstructs.2014.03.015.

[18] Shaaban, Mahmoud and Mohany, Atef. "Synchronous vortex shedding from aerodynamically isolated side-by-side cylinders imposed by flow-excited resonant acoustic modes." *Experiments in Fluids* Vol. 62 (2021): p. 205. DOI 10.1007/s00348-021-03301-9.

[19] Shaaban, Mahmoud and Mohany, Atef. "Phase-resolved PIV measurements of flow over three unevenly spaced cylinders and its coupling with acoustic resonance." *Experiments in Fluids* Vol. 60 (2019): p. 71. DOI 10.1007/s00348-019-2720-7.

[20] Porteous, Ric, Moreau, Danielle J. and Doolan, Con J. "A review of flow-induced noise from finite wall-mounted cylinders." *Journal of Fluids and Structures* Vol. 51 (2014): pp. 240–254. DOI 10.1016/j.jfluidstructs.2014.08.012.

[21] Rashed, Mostafa R., Elsayed, Mostafa E.A. and Shaaban, Mahmoud. "Influence of magnetically-induced nonlinear added stiffness on the lift galloping of square cylinders at low Reynolds number." *Journal of Fluids and Structures* Vol. 124 (2024): p. 104046. DOI 10.1016/j.jfluidstructs.2023.104046.

[22] Buchan, Andrew G., Yang, Liang and Atkinson, Kirk D. "Predicting airborne coronavirus inactivation by far-UVC in populated rooms using a high-fidelity coupled radiation-CFD model." *Scientific Reports* Vol. 10 (2020): p. 19659. DOI 10.1038/s41598-020-76597-y.

[23] Gloerfelt, Xavier, Bailly, Christophe and Juvé, Daniel. "Direct computation of the noise radiated by a subsonic cavity flow and application of integral methods." *Journal of Sound and Vibration* Vol. 266 (2003): pp. 119–146. DOI 10.1016/S0022-460X(02)01531-6.

[24] Mohany, Atef and Ziada, Samir. "Numerical Simulation of the Flow-Sound Interaction Mechanisms of a Single and Two-Tandem Cylinders in Cross-Flow." *Journal of Pressure Vessel Technology* Vol. 131 (2009). DOI 10.1115/1.3110029.

[25] Goldstein, Marvin E. "Aeroacoustics of Turbulent Shear

Copyright © 2024 by ASME

Flows." *Annual Review of Fluid Mechanics* Vol. 16 (1984): pp. 263–285. DOI 10.1146/annurev.fl.16.010184.001403.

[26] Howe, Michael S. "The dissipation of sound at an edge." *Journal of Sound and Vibration* Vol. 70 (1980): pp. 407–411. DOI 10.1016/0022-460X(80)90308-9.

[27] Hong, Zhiliang, Wang, Xiaoyu, Jing, Xiaodong and Sun, Xiaofeng. "Frequency lock-in mechanism in flow-induced acoustic resonance of a cylinder in a flow duct." *Journal of Fluid Mechanics* Vol. 884 (2020): p. A42. DOI 10.1017/jfm.2019.966.

[28] Menter, Florian R. "Two-equation eddy-viscosity turbulence models for engineering applications." *AIAA Journal* Vol. 32 (1994): pp. 1598–1605. DOI 10.2514/3.12149.

[29] Arafa, Nadim, Tariq, Ahmed, Mohany, Atef and Hassan, Marwan. "Effect of cylinder location inside a rectangular duct on the excitation mechanism of acoustic resonance." *Canadian Acoustics* Vol. 42 No. 1 (2014): p. 33 – 40.

[30] Arafa, Nadim and Mohany, Atef. "Flow-Excited Acoustic Resonance of Isolated Cylinders in Cross-Flow." *Journal of Pressure Vessel Technology* Vol. 138 (2016). DOI 10.1115/1.4030270.

[31] Roeck, Wim De and Desmet, Wim. "Accurate CAA-Simulations Using a Low-Mach Aerodynamic/Acoustic Splitting Technique." 2009. American Institute of Aeronautics and Astronautics. DOI 10.2514/6.2009-3230.

[32] Schoder, Stefan, Roppert, Klaus and Kaltenbacher, Manfred. "Postprocessing of Direct Aeroacoustic Simulations Using Helmholtz Decomposition." *AIAA Journal* Vol. 58 (2020): pp. 3019–3027. DOI 10.2514/1.J058836.

[33] Howe, Michael S. *Acoustics of Fluid-Structure Interactions*. Cambridge University Press (1998). DOI 10.1017/CBO9780511662898.

[34] Yoshikawa, Shigeru, Tashiro, Hiromi and Sakamoto, Yumiko. "Experimental examination of vortex-sound generation in an organ pipe: A proposal of jet vortex-layer formation model." *Journal of Sound and Vibration* Vol. 331 (2012): pp. 2558–2577. DOI 10.1016/j.jsv.2012.01.026.

[35] Roache, Patrick J. "Quantification of uncertainty in computational fluid dynamics." *Annual Review of Fluid Mechanics* Vol. 29 (1997): pp. 123–160. DOI 10.1146/annurev.fluid.29.1.123.

[36] Stringer, Robert M., Zang, Jun and Hillis, Andrew J. "Unsteady RANS computations of flow around a circular cylinder for a wide range of Reynolds numbers." *Ocean Engineering* Vol. 87 (2014): pp. 1–9. DOI 10.1016/j.oceaneng.2014.04.017.

Copyright © 2024 by ASME